1 **Calibration of a photoacoustic spectrometer cell using light**

2 **absorbing aerosols. A technical note.**

3

4 Nir Bluvshtein,[1] J. Michel Flores,[1] Quanfu He,[1] Enrico Segre,[2] Lior Segev,[1] Nina Hong,[3] Andrea

5 Donohue,[3] James N. Hilfiker[3] and Yinon Rudich[1,*]

6 [1] Department of Earth and Planetary Sciences, Weizmann Institute of Science, Rehovot 76100, Israel

7 [2] Physical services, Weizmann Institute of Science, Rehovot 76100, Israel

8 [3] J.A. Woollam Co., Inc., 645 M Street, Suite 102 Lincoln, NE 68508, U.S.A.

9 *Correspondence to:* Yinon Rudich (yinon.rudich@weizmann.ac.il)

10

Abstract

12 Multi-pass photoacoustic spectrometer (PAS) is an important tool for the direct measurement of

13 light absorption by atmospheric aerosol. And accurate PAS measurements require an accurate

14 calibration of its signal. Ozone is often used for calibrating the PAS by relating the instrument

15 signal to the absorption coefficient measured by an independent method such as cavity ring down

16 spectroscopy (CRD), cavity enhanced spectroscopy (CES) or an ozone monitor. We report here a

17 calibration method that uses measured absorption coefficients of aerosolized, light absorbing

18 organic materials and offer an alternative approach to calibrate the PAS at 404 nm. To

19 implement this method we first determined the complex refractive index of an organic dye using

20 spectroscopic ellipsometry, and then we use this well characterized material as a standard

21 material for PAS calibration.

22

Introduction

24   Light absorption by atmospheric aerosols still poses one of the greatest uncertainties

25 associated with the effective radiative forcing due to aerosol-radiation interactions (IPCC, 2013).

26 Absorption of incoming solar radiation exerts positive radiative forcing to the top of the

27 atmosphere due to heat transfer from light absorbing aerosols to their surroundings. It may also

28 lead to stagnation and clouds dissipation. In terms of positive radiative forcing, black carbon

29 (BC) aerosols are commonly considered to be second only to CO_2 (Bond et al., 2013) with strong

30 absorption throughout the solar spectrum. Characterization and quantification of light absorbing

31 organic aerosols, referred to as brown carbon (BrC), have been given increasing attention in the

32 past decade (Andreae and Gelencser, 2006; Bond and Bergstrom, 2006; Alexander et al., 2008;

33 Flores et al., 2012b; Lack et al., 2012a; Flores et al., 2014; Laskin et al., 2015; Moise et al.,

34 2015). Although the atmospheric burden of BrC is estimated to be more than three times that of

35 BC (Feng et al., 2013) its absorption is strongly spectral-dependent with strong absorption in the

36 UV and visible spectrum and weak to non-absorbing in the longer wavelengths (Hoffer et al.,

37 2004; Kirchstetter et al., 2004; Kaskaoutis et al., 2007; Sun et al., 2007; Chen and Bond, 2010;

38 Moosmuller et al., 2011; Lack et al., 2012a).

39 Light absorption properties of BrC and its mixing with absorbing and non-absorbing aerosol

40 components introduce a need for sensitive and accurate direct measurement of light absorbing

41 aerosols which is still very challenging. For example, filter based techniques such as the Particle

42 Soot Absorption Photometer (PSAP), the Multi Angle Absorption Photometer (MAAP) and the

43 aethalometer, require correction factors which are based on some *a-priori* information regarding

44 aerosol type and source and have accuracy in the range of 20% to 35% (Bond et al., 1999;

45 Weingartner et al., 2003; Collaud Coen et al., 2010; Muller et al., 2011).

46   Multi-pass photoacoustic spectrometer (PAS) at several wavelengths throughout the visible

47 spectrum has the potential to produce sensitive direct measurements of light absorption due to

48 BrC aerosols. Coupling PAS instruments to a thermal denuder and cavity ring down

49 spectrometers (CRD-S) to measures the absorption and extinction coefficients simultaneously at

50 temperatures ranging from ambient to over 450 ^{0}C allow attribution of aerosol light absorption to

51 BrC, BC, and BC with enhanced absorption due to less-absorbing coating (Cappa et al., 2012;

52 Lack et al., 2012b).

53   In a PAS cell, a modulated laser light is absorbed by a sample of particles or gas, generating

54 a modulated acoustic wave with intensity that is proportional to the energy absorbed by the

55 sample. This acoustic wave, which is detected by a sensitive microphone, has a characteristic

56 radial and longitudinal resonance when the light source is modulated at the cavity resonance

57 frequency (F_r). A more detailed description of the PAS method for aerosol light absorption

58 measurement may be found in Arnott et al., (1999) and Nagele and Sigrist, (2000).

59   While direct, *in-situ* aerosol absorption measurement using PAS avoids the disadvantages of

60 filter based techniques, an accurate calibration procedure is required to relate the instrument

Atmospheric
Measurement
Techniques
Open Access
Discussions

EGU

61   signal to the absorption coefficient (α_{abs}). One way of achieving this is to directly relate the α_{abs}

62   to the microphone response and the laser power by a theoretical relation (Arnott et al., 1999):

$$\alpha_{abs} = \frac{P_{mic}}{P_{Laser}} \frac{A_{res}}{\gamma - 1} \frac{\pi^2 F_r}{Q} \tag{1}$$

$$Q = \frac{F_r}{FWHM} \tag{2}$$

63   where P_{Laser} is absolute laser power in the resonator, A_{res} is resonator cross sectional area, γ is

64   isobaric to isochoric specific heats taken as a constant in dry air, P_{mic} is the microphone signal

65   power, Q is the resonant cavity quality factor and FWHM is the full width half maximum of the

66   acoustic response curve. The F_r and the FWHM are sensitive to temperature, pressure and type of

67   carrier gas.

68   When the laser intensity inside the PAS cell is unknown or when it is not possible to

69   measure, as in the case of an astigmatic cell alignment, the instrument's response needs to be

70   calibrated empirically. This involves comparing the PAS signal to an independent transmittance

71   measurement where scattering is negligible (Arnott et al., 2000; Lack et al., 2006). A common

72   PAS calibration procedure is done by comparing direct measurements of α_{abs} at several

73   concentrations of an absorbing gas by cavity ring down spectrometer (CRD-S) with a parallel

74   measurements by the PAS cell (Lack et al., 2006; Lack et al., 2012b; Lambe et al., 2013). This

75   method is applicable when the Rayleigh scattering by the gas molecules is several orders of

76   magnitude smaller than the absorption and can be neglected. Since gas absorption cross sections

77   can be highly dependent on the wavelength (Vandaele et al., 2002; Bogumil et al., 2003), it is

78   essential to precisely know the wavelength of the light source used in each instrument or to use

79   the same light source in both instruments. At $\lambda = 404$ nm wavelength, $NO_{2(g)}$ is highly absorbing

80   with molecular absorption cross section (σ_{abs}) of 6.12×10^{-19} cm^2 molecule^{-1} (Bogumil et al.,

81   2003). However, at this wavelength NO_2 has a large quantum yield (Φ) of 0.44 (Troe, 2000) and

82   it readily photolyases. Without accurate determination of the laser's power, it is difficult to

83   quantify the photolysis. At the same wavelength, O_3 has the advantage of being stable with Φ

84   approaching zero (Bauer et al., 2000) and it is easily produced on-site or in the laboratory. The

85   disadvantage of O_3 for PAS calibration at $\lambda=404$ nm, is that its σ_{abs} is about 4 orders of

86   magnitude lower than that of NO_2. Different studies reported a wide range of σ_{abs} for O_3 at $\lambda =$

Atmospheric
Measurement
Techniques
Discussions
Open Access
EGU

87   404 nm ranging from 1.5×10^{-23} to 6.3×10^{-23} cm^2 molecule^{-1} (Burrows et al., 1999; Voigt et al.,

88   2001; Bogumil et al., 2003; Axson et al., 2011) (Figure 1). For this reason, O_3 calibration

89   requires very high concentration (in the order of 100's to 1000's ppmv) which may cause

90   equipment degradation. An additional concern is that at concentrations in the order of 1000's

91   ppmv, O_3 may change the F_r of the PAS cell. The extent of this effect depends on the O_3

92   concentration and on the instruments' sensitivity to gas composition i.e. the Q, and it can also be

93   easily calculated using a simple thermodynamic model for the speed of sound. In such a case the

94   laser modulation frequency should be adjusted to the new F_r value.

95   An alternative calibration method is to use a standard aerosol with well-known absorption

96   properties. PAS calibration using size selected light absorbing particles requires a standard

97   material with accurate information of its complex refractive index at the instrument's

98   wavelength, which is not widely available. This procedure is also time consuming in comparison

99   to the use of a light absorbing gas and may be more difficult to implement on field and aircraft

100   applications.

101   Lack et al., (2012b), reported the development of the current PAS instrument. They

102   calibrated their PA-CRD-S (PAS coupled to a CRD-S) cells at 405 nm and at 532 nm with O_3

103   and commented that NO_2 calibration at 405 nm is possible using a photolysis correction factor

104   for the CRD-S measurements. Several other publications used the same instruments as in Lack et

105   al., (2012b) using O_3 calibration procedure (Cappa et al., 2012; Lack et al., 2012a; Lambe et al.,

106   2013).

107   Using a similar PAS cell as Lack et al., (2012b), we attempted to measure α_{abs} and

108   extinction coefficients (α_{ext}) of brown carbon (BrC) proxy materials using the PA-CRD-S

109   following calibration of the PAS using O_3. The results yielded very high α_{abs} values which were

110   not consistent with other measurements. Therefore, we developed a reliable procedure to

111   calibrate the PAS instrument using light absorbing particles produced in the laboratory with a

112   widely available water soluble absorbing material – nigrosin. In this study, we describe the

113   details of this procedure which includes high accuracy measurement of the nigrosin complex

114   refractive index (RI) using spectroscopic ellipsometry. We also show that there are significant

115   differences between the PAS response curve calculated using nigrosin particles and the PAS

116   response curve calculated using O_3.

Atmospheric
Measurement
Techniques
Open Access
Discussions

EGU

Methodology

Photoacoustic aerosol spectrometer

119   The multi-pass astigmatic PAS cell that is used in this work is described in Lack et al.,

120   (2012b) and only a brief description is given here. It is composed of dual half-wavelength

121   resonators (11 cm long, 1.9 cm diameter) capped on either end with 1/4 wavelength acoustic

122   notches. The total sample cell volume is 185 cm^3. While both resonators are open to the sample

123   flow, only one is exposed to the modulated laser light; the other is planned for noise cancellation.

124   Microphones are placed at the antinode of the sound wave in the center of each resonator and the

125   speaker is placed at the background resonator. The F_r of the system is found by producing 1 sec

126   segments of white noise using the speaker located in the reference resonator. Each segment is

127   sampled by the microphones at a 100 kHz rate and the F_r is found by performing a Fast Fourier

128   Transform. Examples of power spectra with different carrier gas compositions are shown in

129   Figure 2 were F_r is the frequency at the peak of the fitted Lorentzian curve. Typical Fr and Q

130   values for our instrument are in the range of 1360–1385 Hz and 40-50 (unitless), respectively,

131   over the pressure (97–101 kPa), relative humidity (RH; 0 - 11% RH) and temperature (20 to 24

132   °C) ranges, and with two carrier gases (N_2 or synthetic air). The instrument described in Lack et

133   al., (2012b) produced an F_r in the range of 1320 to 1360 Hz, Q in the range of 50 to 90 over

134   pressure and temperature ranges of 20 to 90 kPa and 12 to 23 ^{o}C when dried air was used as

135   carrier gas.

136   The astigmatic optical configuration consists of two high reflectivity mirrors (ARW Optical,

137   Wilmington, NC, USA; dielectric coating R > 99.5%), 1.5" diameter, spaced 35 cm apart. The

138   laser side mirror has a cylindrical radius of curvature of 43 cm and a 2 mm hole drilled in the

139   center. The back mirror has a cylindrical radius of curvature of 47 cm, and is rotated 90° to the

140   radius of curvature of the laser side mirror. Astigmatic alignment is achieved by aligning the

141   laser through the 2 mm hole drilled in the center of the first mirror and on to an off-center target

142   on the second mirror. Each following reflection is also directed to an off-center target on the

143   opposite mirror. Each mirror was placed on kinematic mirror mounts for easy alignment

144   (KM200, with an AD2-1.5 adaptor; Thorlabs, U.S.A). The PAS cell is mounted within the path

145   of the laser multi-pass and is covered by 50 mm thick acoustic foam. The laser light passes

Atmospheric
Measurement
Techniques
Discussions

146   through the PAS cell through two 1 mm thick windows (CVI Laser, Albuquerque, NM, USA),

147   each with a high transmissivity (T > 99.5%) antireflective coating.

Cavity ring down spectrometer

149   A detailed description of the CRD-S method for aerosol light extinction measurement may be

150   found in Pettersson et al., (2004), Abo Riziq et al., (2007), Smith and Atkinson, (2001),

151   Bluvshtein et al., (2012) and references therein. The CRD-S used in this study differs from the

152   one described in a previous publication (Bluvshtein et al., 2012). Here the laser modulation rate

153   is varied to meet the PAS cell F_r. The cavity length and the aerosol filled length were extended to

154   95 and 80 cm respectively. Additionally, the gas/aerosol inlet to the cavity was moved to the

155   center of the cavity with two outlets at the cavity sides (Figure 3) from which the gas/aerosols

156   are pulled out. In this configuration the uncertainty associated with the ratio of cavity length to

157   aerosol filled length is reduced significantly regardless of flow conditions (i.e. ratio of sample

158   flow to mirror purge flow and cavity inner diameter). Discussion on errors associated with R_L

159   uncertainty may be found in Miles et al., (2011) and Toole et al., (2013).

Photoacoustic aerosol spectrometer coupled to a cavity ring down aerosol spectrometer

161   The photoacoustic aerosol spectrometer coupled to a cavity ring down aerosol spectrometer

162   (PA-CRD-S) described in this section (Figure 3) is composed of a 110 mW 404 nm diode laser

163   (iPulse, Toptica Photonics, Germany) modulated in the measured PAS resonance frequency at

164   50% duty cycle. The laser beam is split into two separate optical paths (CRD-S and PAS) using a

165   variable polarized beam splitter. The beam splitter is composed of a quarter waveplate (¼λ) and

166   a polarizing beam splitter (PBS). With the current setup, turning the ¼λ between 0 and 90° varies

167   the intensity ratio between the two optical paths from 0:1 to 1:1 CRD-S to PAS optical path,

168   respectively. The beam directed to the PAS is turned and aligned into the PAS cell through a set

169   of two plano-convex lenses (focal lengths of 30 mm and 50 mm) used as a telescope in order to

170   collimate the beam into a diameter of about 1.5 mm. The beam, directed to the CRD-S, passes

171   through another ¼λ plate, which together with the PBS serves as a variable attenuator protecting

172   the laser head from the beam reflected backwards by the CRD-S highly reflective mirror. This

173   back-reflected beam (dashed arrow in Figure 3) is transmitted through the PBS and is detected

174   by a photodiode and is used as an external trigger source for the CRD-S intensity decay

175   measurement. The forward beam is then turned and aligned into the CRD-S cavity by a set of

Atmospheric
Measurement
Techniques
Open Access
Discussions
EGU

176   turning mirrors. While the PAS sensitivity depends on the laser power, the CRD-S system

177   requires only the minimal laser power needed by the photodiode. This allowed us to divert

178   approximately 78% of the laser power (about 86 mW) to the PAS cell and thus optimize its

179   sensitivity.

180   **PAS calibration**

181   To calibration the PAS cell, gas flow was pulled and split between the PAS and the CRD-

182   S at a flow ratio of 3:1 to equal the volume ratio of the two instruments. O_3 was generated by a

183   constant flow of high purity (99.999%) O_2 through a UV lamp O_3 generator (model 300, Jelight

184   Company, Inc. CA, U.S.A) for up to 800 ppm O_3 and through a corona discharge ozone

185   generator (model L21, Pacific Ozone, CA, U.S.A) for up to 4000 ppm O_3. The O_3 out flow was

186   mixed with dry N_2 to a 90% N_2 10% O_2/O_3 mixture. The O_3 concentrations were varied by

187   adjusting the height of the cover glass of the UV lamp O_3 generator and by adjusting the voltage

188   gauge of the corona discharge ozone generator. At each gas concentration, data were acquired at

189   a rate of 1 Hz and averaged over intervals of two minutes.

190   **Measurement of the complex refractive index of nigrosin by Spectroscopic ellipsometry**

191   To infer the complex refractive index (RI) of nigrosin at $\lambda = 404$ nm from ellipsometry

192   measurements, five silicon wafers (surface area - 4 cm^2) with 300 nm of silicon thermal oxide

193   (Virginia Semiconductor, VA, U.S.A) were coated with nigrosine using concentrated aqueous

194   solutions and a spin coater (WS-400A-6NPP/LITE; Laurell Technologies Corporation, PA,

195   U.S.A). The concentration of the nigrosin solution was 1.25 and 1.5 times the room temperature

196   solubility limit of nigrosin (10 gr L^{-1}) and was kept at 40°C under constant stirring to maintain

197   solubility. Spin coating was done in two stages, a coating stage and a drying stage. During the

198   coating stage each sample was covered by the nigrosin solution and the spinning was done at

199   100, 500 or 700 RPM under dry N_2 flow for 14 minutes. The drying stage was performed at 3500

200   rpm for 1 minute in order to reach complete dryness and to remove liquid droplets adhering to

201   the wafer edges. Dry N_2 flowed from below the wafer stage in an upward direction so it will not

202   affect the liquid spreading on the wafer.

203   Spectroscopic ellipsometry is a proven method to determine thin film thickness and

204   complex refractive index (m = n + ik) of materials (Fujiwara, 2007). Briefly, ellipsometry uses

205   polarized light to characterize thin film and bulk materials. A change in the electric field

206   amplitude and phase for p- and s- polarizations is measured after reflecting light from the

207   surface. Thin film thickness and optical constants (n and k) are derived from the measurement.

208   Spectroscopic ellipsometry measurements were performed on the five film samples (described

209   above) using a J.A. Woollam M-2000 DI ellipsometer in the spectral range of 193 nm to 1700

210   nm at angles of incidence of 55°, 65°, and 75°. The instrument was pre-calibrated with a

211   calibration wafer to minimize systematic errors that are related to angle, wavelength and delta

212   offsets. In case of light absorbing materials k is often correlated with the sample thickness. To

213   overcome this issue, we employed the interference enhancement technique to improve sensitivity

214   to light absorption as described in Hilfiker et al., (2008). The resulting film optical constants

215   were evaluated by comparison with the optical constants obtained from a simultaneous analysis

216   of all five samples (multi-sample analysis; MSA). With the two methods, we obtained high

217   sensitivity to light absorption. The Kramers-Kronig consistent complex refractive index of the

218   nigrosin films was modeled using five Gaussian oscillators along with a Sellmeier function. The

219   best-fit model was determined by the Levenberg-Marquardt regression algorithm and tested for

220   both statistical errors and model systematic errors. Statistical errors were estimated by the

221   Bootstrap re-sampling method (Rosa, 1988) and the model systematic errors were estimated

222   using the difference between the measured data and the best-fit model generated data.

PAS calibration with measurements of nigrosin aerosol

224   A nigrosin solution was atomized, and the resulting aerosol dried, size selected (250 nm

225   to 325 nm at 25 nm steps) (Bluvshtein et al., 2012; Flores et al., 2012a) and the absorption signal

226   was measured with the PAS instrument at several number concentrations (counted by a

227   condensation particle counter; CPC). Size selection was performed using an electrostatic

228   classifier (3080L, TSI, MN, U.S.A) equipped with an impactor (nozzle diameter of 457 μm).

229   Sample flow was set between 1 to 0.7 LPM such that the 50% cut-off diameter of the impactor

230   was 50 nm above the selected size. The impactor was used to reduce multiply charged particles

231   contribution. The signal of the PAS was compared to the aerosol α_{abs} calculated using Mie theory

232   algorithm from the complex RI retrieved from the dry film SE measurements together with the

233   particles number concentration.

Atmospheric
Measurement
Techniques
Discussions

Results

235   Figure 4 shows the result of a single sample and a multi-sample analysis of the spectroscopic

236   ellipsometry complex RI retrieval, at 300 nm to 800 nm range. The single sample analysis shown

237   was performed on the sample with the thickest retrieved nigrosin film (137.2 ± 0.3 nm, coated

238   with 15 gr L^{-1} nigrosin solution at 100 RPM). The imaginary part from the SE analysis is in good

239   agreement with the imaginary part calculated from aqueous solution UV-Vis absorption

240   measurement (Sun et al., 2007). The density of nigrosin for this calculation was taken as 1.6 gr

241   cm^{-3} (Moteki et al., 2010). The complex RI of nigrosin at λ = 404 nm was determined by the

242   spectroscopic ellipsometry analysis to be m = 1.624 (±0.008) + i 0.154 (±0.008). The summed

243   precision and accuracy of the retrieved complex RI are about 0.5% for n and 5% for k. Figure 4

244   also shows previously published complex RI values for nigrosin retrieved at 532 nm and 355 nm

245   wavelengths using CRD-S (Lack et al., 2006; Dinar et al., 2008; Lang-Yona et al., 2009;

246   Bluvshtein et al., 2012; Flores et al., 2012a). Such wide spread of complex RI values emphasizes

247   the need for a more accurate measurement for future use of nigrosin as a standard material, and

248   the limitations of the CRD method, that can benefit from a new well-established standard.

249   To further verify the validity of the new calibration approach we have used Pahokee peat

250   fulvic acid (PPFA) and Suwannee river fulvic acid (SRFA) which are often used as a proxy

251   material for atmospheric brown carbon due to their complex organic composition and their UV-

252   Vis absorption spectrum. In an accompanying paper Bluvshtein et al., showed that the mass

253   absorption cross section (MAC) of PPFA and SRFA, calculated from UV-Vis aqueous solution

254   absorption spectrum, is within the value range of the MAC calculated for ambient water soluble

255   organic aerosol collected during a biomass burning event.

256   Size selected PPFA and SRFA particles were measured with the PA-CRD-S and the complex

257   RI was retrieved from the CRD-S measurements using a Mie theory algorithm taking into

258   account the multiply charged particles (MCP) contribution (Flores et al., 2012a; Washenfelder et

259   al., 2013; Bluvshtein et al., 2016). The imaginary part of the complex RI was also calculated

260   from UV-Vis aqueous solution absorption measurement using material density estimation of 1.1

261   to 1.3 gr cm^{-3}. Our best estimation of the complex RI of PPFA and SRFA at λ = 404 nm are m =

262   1.699 (±0.012) + i 0.036 (±0.010) and m = 1.685 (±0.020) + i 0.013 (±0.010) respectively. This

263   information together with the measured particle number concentration and MCP contribution

Atmospheric
Measurement
Techniques
Discussions

264 was used to calculate α_{abs} using Mie theory. Calculated α_{abs} of PPFA and SRFA are plotted

265 against the measured PAS signal in Figure 5. In addition, Figure 5 shows an O_3 calibration curve

266 with a slope of 4.975×10^{-7} cm^{-1} V^{-1} and a nigrosin calibration curve with a slope of 2.533×10^{-7}

267 cm^{-1} V^{-1}. Figure 5 clearly demonstrates that the PAS response curves calculated for the three

268 types of organic aerosols agree with each other, while the slope of the response curve produced

269 with O_3 over-estimates the instrument's response by a factor of about two. This implies that

270 measurements of aerosols α_{abs} at $\lambda = 404$ using PAS calibrated with O_3 may be significantly over

271 estimated.

272 With a parallel flow configuration, higher loss of $O_{3(g)}$ molecules to the PAS (aluminum)

273 walls in comparison to the CRD-S walls (stainless steel and lower surface to volume ratio) would

274 result in an underestimation of the PAS response and an overestimation of the calibration slope.

275 A similar artifact could result from reaction of the $O_{3(g)}$ with residual aerosol material on the

276 CRD-S walls, producing ultra-fine light scattering particles. These particles, if produced would

277 increase the CRD-S α_{ext} and cause an overestimation of the calibration slope. Repetitions of the

278 calibration procedure in tandem flow configuration, linearity and repeatability of the calibration

279 curve and the stability of the CRD-S signal ruled-out these affects as possible causes for the

280 overestimation of the PAS response due to the $O_{3(g)}$ calibration procedure.

281 Additionally, we did not find any literature information regarding significant energy

282 relaxation processes following UV-Vis light absorption by $O_{3(g)}$ which do not involve thermal

283 conversion.

284 **Conclusion**

285 In this study we demonstrate a new calibration for PAP instrument using nigroisn, a widely

286 available water-soluble absorbing material. We have derived the complex refractive index of

287 nigrosin throughout the UV and visible range using spectroscopy ellipsometry and suggest that it

288 can now be used as a standard material to calibrate PAS instruments at the UV-Vis-NIR

289 wavelength range for measurements of light absorbing aerosols. Nigrosin can also be used to

290 validate other chosen PAS calibration procedures. Our measurements also imply that calibration

291 of PAS with O_3 at 404 nm may lead to over-estimation of light absorption by aerosol.

Atmospheric
Measurement
Techniques
Discussions

Open Access

EGU

292   As shown in this study, spectroscopic ellipsometry may be used to accurately determine the

293   complex RI of other organic dyes that may be used for the same purpose. It requires, however,

294   the production of uniform films of the studied material.

295   **Figures**
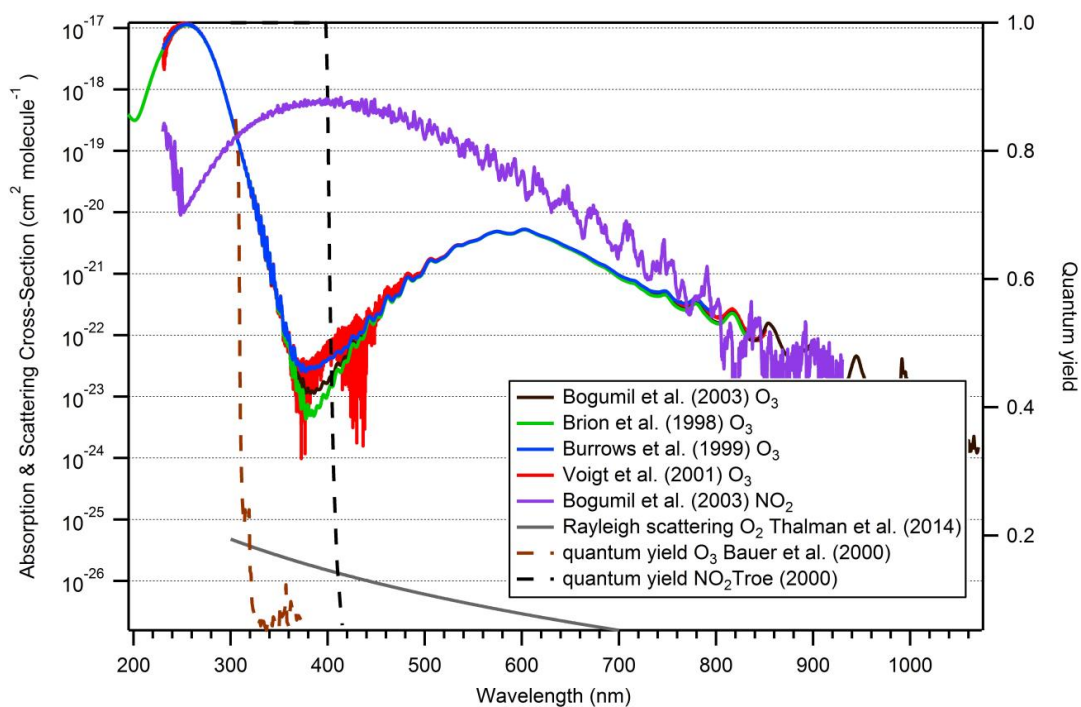
296

297   Figure 1: Spectral absorption cross-sections and quantum yields of O_3 and NO_2.

Atmospheric
Measurement
Techniques

Discussions
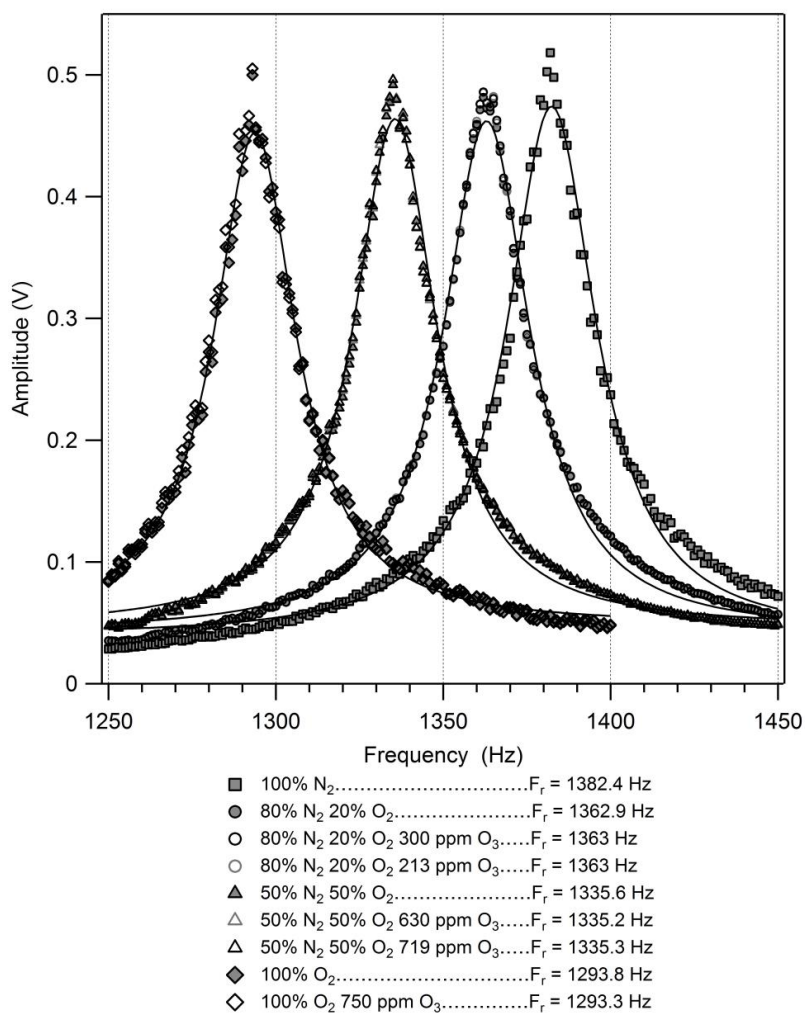
298

299   Figure 2: Fast Fourier transform (FFT) resultant power spectra with different carrier gas composition and O_3

300   concentration. O_3 was measured downstream to the PAS using the CRD-S assuming O_3 σ_{abs} of 1.5×10^{-23} cm^2

301    $molecule^{-1}$ from Axson et al., (2011).

302

Atmospheric
Measurement
Techniques
Discussions

303
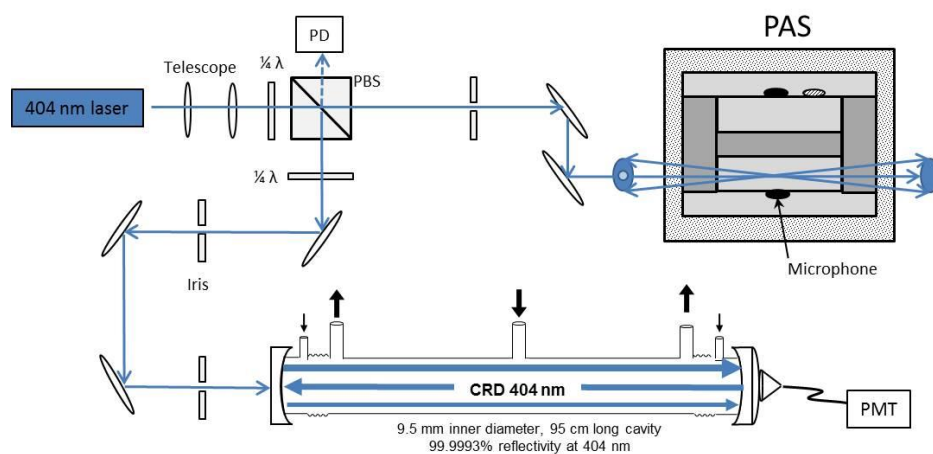
Figure 3: Schematic of the photo-acoustic spectrometer (PAS) coupled to a cavity ring down (CRD) spectrometer (PA-CRD-S). Abbreviations: PBS, polarizing beam splitter; PD, photodiode; PMT, photomultiplier tube. Small black arrows indicate the entrance of the purge flows, and the thinker black arrows the direction of the aerosol flow (Bluvshtein et al., 2016).
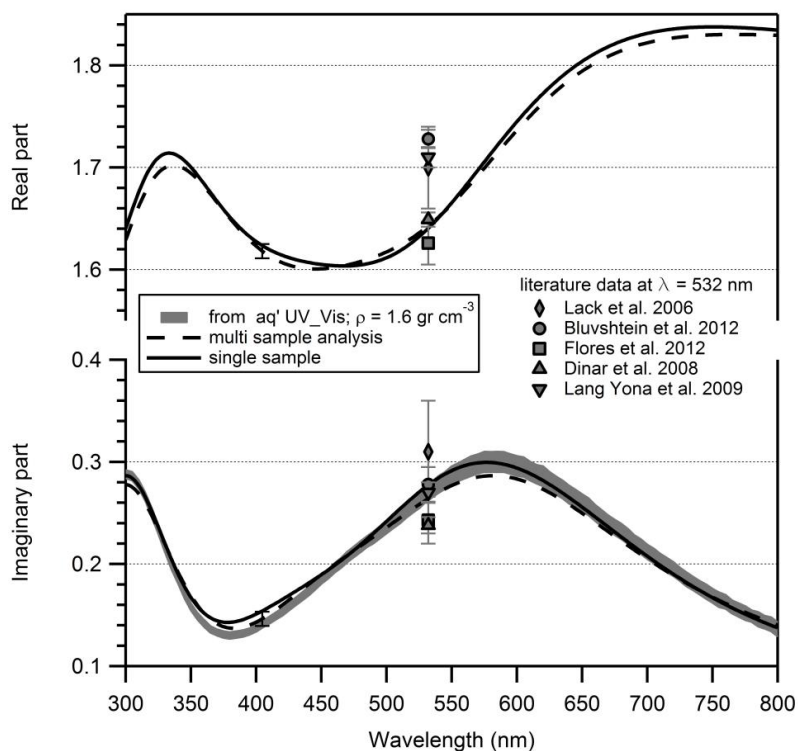
308

309 Figure 4: Complex RI results of spectroscopic ellipsometry measurements of nigrosin coating on Si oxide. Also

310 shown are results of imaginary part calculated from aqueous UV-Vis measurements based on Sun et al., (2007) with

311 density value of 1.6 gr cm^{-3} (Moteki et al., 2010).
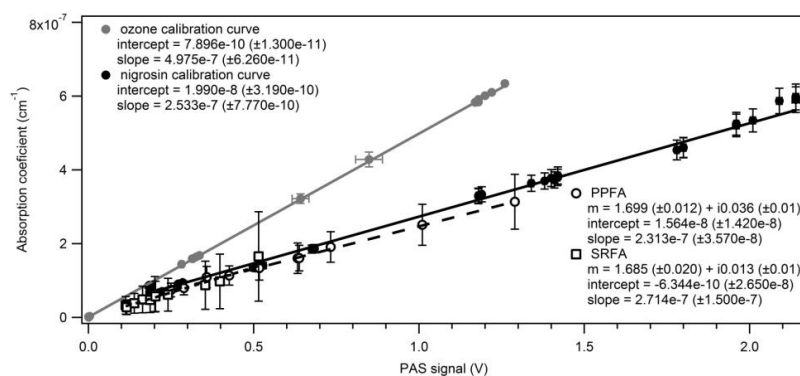
312

313 Figure 5: PAS O$_3$ calibration curve and regression (gray), nigrosin calibration curve and regression based on SE

314 analysis (black circles and line) and PPFA and SRFA based on complex RI retrieval from CRD-S measurements and

315 aqueous UV-Vis measurements.

References

317 Abo Riziq, A., Erlick, C., Dinar, E., and Rudich, Y.: Optical properties of absorbing and non-
318 absorbing aerosols retrieved by cavity ring down (crd) spectroscopy, Atmos Chem Phys, 7,
319 1523-1536, 2007.

320

321 Alexander, D. T., Crozier, P. A., and Anderson, J. R.: Brown carbon spheres in east asian
322 outflow and their optical properties, Science, 321, 10.1126/science.1155296, 2008.

323

324 Andreae, M. O., and Gelencser, A.: Black carbon or brown carbon? The nature of light-
325 absorbing carbonaceous aerosols, Atmos. Chem. Phys., 6, 10.5194/acp-6-3131-2006, 2006.

326

327 Arnott, W. P., Moosmuller, H., Rogers, C. F., Jin, T. F., and Bruch, R.: Photoacoustic
328 spectrometer for measuring light absorption by aerosol: Instrument description, Atmos. Environ.,
329 33, 10.1016/s1352-2310(98)00361-6, 1999.

330

331 Arnott, W. P., Moosmuller, H., and Walker, J. W.: Nitrogen dioxide and kerosene-flame soot
332 calibration of photoacoustic instruments for measurement of light absorption by aerosols, 71,
333 10.1063/1.1322585, 2000.

334

Atmospheric
Measurement
Techniques
Open Access
Discussions
EGU

335 Axson, J. L., Washenfelder, R. A., Kahan, T. F., Young, C. J., Vaida, V., and Brown, S. S.:
336 Absolute ozone absorption cross section in the huggins chappuis minimum (350–470 nm) at 296
337 k, 11, 10.5194/acp-11-11581-2011, 2011.

338

339 Bauer, D., D'Ottone, L., and Hynes, A. J.: O 1d quantum yields from o3 photolysis in the near uv
340 region between 305 and 375 nm, 2, 10.1039/B000159G, 2000.

341

342 Bluvshtein, N., Flores, J. M., Riziq, A. A., and Rudich, Y.: An approach for faster retrieval of
343 aerosols' complex refractive index using cavity ring-down spectroscopy, Aerosol. Sci. Tech., 46,
344 10.1080/02786826.2012.700141, 2012.

345

346 Bluvshtein, N., Flores, J. M., Segev, L., and Rudich, Y.: A new approach for retrieving the uv–
347 vis optical properties of ambient aerosols, Atmos. Meas. Tech., 9, 10.5194/amt-9-3477-2016,
348 2016.

349

350 Bogumil, K., Orphal, J., Homann, T., Voigt, S., Spietz, P., Fleischmann, O. C., Vogel, A.,
351 Hartmann, M., Kromminga, H., Bovensmann, H., Frerick, J., and Burrows, J. P.: Measurements
352 of molecular absorption spectra with the sciamachy pre-flight model: Instrument characterization
353 and reference data for atmospheric remote-sensing in the 230–2380 nm region, 157,
354 http://dx.doi.org/10.1016/S1010-6030(03)00062-5, 2003.

355

356 Bond, T. C., Anderson, T. L., and Campbell, D.: Calibration and intercomparison of filter-based
357 measurements of visible light absorption by aerosols, Aerosol Sci Tech, 30, Doi
358 10.1080/027868299304435, 1999.

359

360 Bond, T. C., and Bergstrom, R. W.: Light absorption by carbonaceous particles: An investigative
361 review, Aerosol Sci. Tech., 40, Doi 10.1080/02786820500421521, 2006.

362

363 Bond, T. C., Doherty, S. J., Fahey, D. W., Forster, P. M., Berntsen, T., DeAngelo, B. J., Flanner,
364 M. G., Ghan, S., Karcher, B., Koch, D., Kinne, S., Kondo, Y., Quinn, P. K., Sarofim, M. C.,
365 Schultz, M. G., Schulz, M., Venkataraman, C., Zhang, H., Zhang, S., Bellouin, N., Guttikunda,
366 S. K., Hopke, P. K., Jacobson, M. Z., Kaiser, J. W., Klimont, Z., Lohmann, U., Schwarz, J. P.,
367 Shindell, D., Storelvmo, T., Warren, S. G., and Zender, C. S.: Bounding the role of black carbon
368 in the climate system: A scientific assessment, J Geophys Res-Atmos, 118, 10.1002/jgrd.50171,
369 2013.

370

371 Burrows, J. P., Richter, A., Dehn, A., Deters, B., Himmelmann, S., Voigt, S., and Orphal, J.:
372 Atmospheric remote-sensing reference data from gome—2. Temperature-dependent absorption
373 cross sections of o3 in the 231–794nm range, 61, http://dx.doi.org/10.1016/S0022-
374 4073(98)00037-5, 1999.

375

Atmospheric
Measurement
Techniques
Discussions

376   Cappa, C. D., Onasch, T. B., Massoli, P., Worsnop, D. R., Bates, T. S., Cross, E. S., Davidovits,
377   P., Hakala, J., Hayden, K. L., Jobson, B. T., Kolesar, K. R., Lack, D. A., Lerner, B. M., Li, S.
378   M., Mellon, D., Nuaaman, I., Olfert, J. S., Petaja, T., Quinn, P. K., Song, C., Subramanian, R.,
379   Williams, E. J., and Zaveri, R. A.: Radiative absorption enhancements due to the mixing state of
380   atmospheric black carbon, Science, 337, 10.1126/science.1223447, 2012.

381

382   Chen, Y., and Bond, T. C.: Light absorption by organic carbon from wood combustion, Atmos.
383   Chem. Phys., 10, 1773-1787, 2010.

384

385   Collaud Coen, M., Weingartner, E., Apituley, A., Ceburnis, D., Fierz-Schmidhauser, R., Flentje,
386   H., Henzing, J. S., Jennings, S. G., Moerman, M., Petzold, A., Schmid, O., and Baltensperger,
387   U.: Minimizing light absorption measurement artifacts of the aethalometer: Evaluation of five
388   correction algorithms, 3, 10.5194/amt-3-457-2010, 2010.

389

390   Dinar, E., Riziq, A. A., Spindler, C., Erlick, C., Kiss, G., and Rudich, Y.: The complex refractive
391   index of atmospheric and model humic-like substances (hulis) retrieved by a cavity ring down
392   aerosol spectrometer (crd-as), Faraday Discuss, 137, 10.1039/b703111d, 2008.

393

394   Feng, Y., Ramanathan, V., and Kotamarthi, V. R.: Brown carbon: A significant atmospheric
395   absorber of solar radiation?, Atmos. Chem. Phys., 13, 10.5194/acp-13-8607-2013, 2013.

396

397   Flores, J. M., Bar-Or, R. Z., Bluvshtein, N., Abo-Riziq, A., Kostinski, A., Borrmann, S., Koren,
398   I, Koren, I., and Rudich, Y.: Absorbing aerosols at high relative humidity: Linking hygroscopic
399   growth to optical properties, Atmos. Chem. Phys., 12, 10.5194/acp-12-5511-2012, 2012a.

400

401   Flores, J. M., Bar-Or, R. Z., Bluvshtein, N., Abo-Riziq, A., Kostinski, A., Borrmann, S., Koren,
402   I., and Rudich, Y.: Absorbing aerosols at high relative humidity: Closure between hygroscopic
403   growth and optical properties, 12, 10.5194/acpd-12-1019-2012, 2012b.

404

405   Flores, J. M., Washenfelder, R. A., Adler, G., Lee, H. J., Segev, L., Laskin, J., Laskin, A.,
406   Nizkorodov, S. A., Brown, S. S., and Rudich, Y.: Complex refractive indices in the near-
407   ultraviolet spectral region of biogenic secondary organic aerosol aged with ammonia, Phys.
408   Chem. Chem. Phys., 16, 10.1039/c4cp01009d, 2014.

409

410   Fujiwara, H.: Introduction to spectroscopic ellipsometry, in: Spectroscopic ellipsometry, John
411   Wiley & Sons, Ltd, 1-11, 2007.

412

413   Hilfiker, J. N., Singh, N., Tiwald, T., Convey, D., Smith, S. M., Baker, J. H., and Tompkins, H.
414   G.: Survey of methods to characterize thin absorbing films with spectroscopic ellipsometry, Thin
415   Solid Films, 516, 10.1016/j.tsf.2008.04.060, 2008.

416

417   Hoffer, A., Kiss, G., Blazso, M., and Gelencser, A.: Chemical characterization of humic-like
418   substances (hulis) formed from a lignin-type precursor in model cloud water, Geophys. Res.
419   Lett., 31, Artn L06115

420   Doi 10.1029/2003gl018962, 2004.

421

422   IPCC: Climate change 2013: The physical science basis. Contribution of working group i to the
423   fifth assessment report of the intergovernmental panel on climate change, Cambridge University
424   Press, Cambridge, United Kingdom and New York, NY, USA, 1535 pp., 2013.

425

426   Kaskaoutis, D. G., Kambezidis, H. D., Hatzianastassiou, N., Kosmopoulos, P. G., and
427   Badarinath, K. V. S.: Aerosol climatology: Dependence of the angstrom exponent on wavelength
428   over four aeronet sites, 2007, 10.5194/acpd-7-7347-2007, 2007.

429

430   Kirchstetter, T. W., Novakov, T., and Hobbs, P. V.: Evidence that the spectral dependence of
431   light absorption by aerosols is affected by organic carbon, J. Geophys. Res.-Atmos., 109, Artn
432   D21208 10.1029/2004jd004999, 2004.

433

434   Lack, D. A., Lovejoy, E. R., Baynard, T., Pettersson, A., and Ravishankara, A. R.: Aerosol
435   absorption measurement using photoacoustic spectroscopy: Sensitivity, calibration, and
436   uncertainty developments, Aerosol. Sci. Tech., 40, 10.1080/02786820600803917, 2006.

437

438   Lack, D. A., Langridge, J. M., Bahreini, R., Cappa, C. D., Middlebrook, A. M., and Schwarz, J.
439   P.: Brown carbon and internal mixing in biomass burning particles, Proc. Nat. Acad. Sci. U.S.A.,
440   109, 10.1073/pnas.1206575109, 2012a.

441

442   Lack, D. A., Richardson, M. S., Law, D., Langridge, J. M., Cappa, C. D., McLaughlin, R. J., and
443   Murphy, D. M.: Aircraft instrument for comprehensive characterization of aerosol optical
444   properties, part 2: Black and brown carbon absorption and absorption enhancement measured
445   with photo acoustic spectroscopy, Aerosol. Sci. Tech., 46, 10.1080/02786826.2011.645955,
446   2012b.

447

448   Lambe, A. T., Cappa, C. D., Massoli, P., Onasch, T. B., Forestieri, S. D., Martin, A. T.,
449   Cummings, M. J., Croasdale, D. R., Brune, W. H., Worsnop, D. R., and Davidovits, P.:
450   Relationship between oxidation level and optical properties of secondary organic aerosol,
451   Environ. Sci. Technol., 47, 10.1021/es401043j, 2013.

452

453   Lang-Yona, N., Rudich, Y., Segre, E., Dinar, E., and Abo-Riziq, A.: Complex refractive indices
454   of aerosols retrieved by continuous wave-cavity ring down aerosol spectrometer, Anal. Chem.,
455   81, 10.1021/ac8017789, 2009.

Atmospheric
Measurement
Techniques
Discussions

Open Access

EGU

456

457 Laskin, A., Laskin, J., and Nizkorodov, S. A.: Chemistry of atmospheric brown carbon, Chem.
458 Rev., 115, 10.1021/cr5006167, 2015.

459

460 Miles, R. E. H., Rudic, S., Orr-Ewing, A. J., and Reid, J. P.: Sources of error and uncertainty in
461 the use of cavity ring down spectroscopy to measure aerosol optical properties, Aerosol. Sci.
462 Tech., 45, 10.1080/02786826.2011.596170, 2011.

463

464 Moise, T., Flores, J. M., and Rudich, Y.: Optical properties of secondary organic aerosols and
465 their changes by chemical processes, Chem. Rev., 115, 10.1021/cr5005259, 2015.

466

467 Moosmuller, H., Chakrabarty, R. K., Ehlers, K. M., and Arnott, W. P.: Absorption angstrom
468 coefficient, brown carbon, and aerosols: Basic concepts, bulk matter, and spherical particles,
469 Atmos. Chem. Phys., 11, 10.5194/acp-11-1217-2011, 2011.

470

471 Moteki, N., Kondo, Y., Nakayama, T., Kita, K., Sahu, L. K., Ishigai, T., Kinase, T., and
472 Matsumi, Y.: Radiative transfer modeling of filter-based measurements of light absorption by
473 particles: Importance of particle size dependent penetration depth, J Aerosol Sci, 41,
474 10.1016/j.jaerosci.2010.02.002, 2010.

475

476 Muller, T., Henzing, J. S., de Leeuw, G., Wiedensohler, A., Alastuey, A., Angelov, H., Bizjak,
477 M., Coen, M. C., Engstrom, J. E., Gruening, C., Hillamo, R., Hoffer, A., Imre, K., Ivanow, P.,
478 Jennings, G., Sun, J. Y., Kalivitis, N., Karlsson, H., Komppula, M., Laj, P., Li, S. M., Lunder, C.,
479 Marinoni, A., dos Santos, S. M., Moerman, M., Nowak, A., Ogren, J. A., Petzold, A., Pichon, J.
480 M., Rodriquez, S., Sharma, S., Sheridan, P. J., Teinila, K., Tuch, T., Viana, M., Virkkula, A.,
481 Weingartner, E., Wilhelm, R., and Wang, Y. Q.: Characterization and intercomparison of aerosol
482 absorption photometers: Result of two intercomparison workshops, Atmos Meas Tech, 4,
483 10.5194/amt-4-245-2011, 2011.

484

485 Nagele, M., and Sigrist, M. W.: Mobile laser spectrometer with novel resonant multipass
486 photoacoustic cell for trace-gas sensing, Appl. Phys. B-Lasers. O., 70, 10.1007/PL00021151,
487 2000.

488

489 Pettersson, A., Lovejoy, E. R., Brock, C. A., Brown, S. S., and Ravishankara, A. R.:
490 Measurement of aerosol optical extinction at 532nm with pulsed cavity ring down spectroscopy,
491 j. Aerosol. Sci., 35, 10.1016/j.jaerosci.2004.02.008, 2004.

492

493 Rosa, R.: The inverse problem of ellipsometry: A bootstrap approach, 4, 887, 1988.

494

495 Smith, J. D., and Atkinson, D. B.: A portable pulsed cavity ring-down transmissometer for
496 measurement of the optical extinction of the atmospheric aerosol, The Analyst, 126, 1216-1220,
497 2001.

498

499 Sun, H. L., Biedermann, L., and Bond, T. C.: Color of brown carbon: A model for ultraviolet and
500 visible light absorption by organic carbon aerosol, Geophys. Res. Lett., 34, Artn L17813 Doi
501 10.1029/2007gl029797, 2007.

502

503 Toole, J. R., Renbaum-Wolff, L., and Smith, G. D.: A calibration technique for improving
504 refractive index retrieval from aerosol cavity ring-down spectroscopy, Aerosol Sci Tech, 47,
505 10.1080/02786826.2013.805875, 2013.

506

507 Troe, J.: Are primary quantum yields of no2 photolysis at lambda <= 398 nm smaller than
508 unity?, Z. Phys. Chemie-Int. J. Res. Phys. Chem. Chem. Phys., 214,
509 10.1524/zpch.2000.214.5.573, 2000.

510

511 Vandaele, A. C., Hermans, C., Fally, S., Carleer, M., Colin, R., Mérienne, M. F., Jenouvrier, A.,
512 and Coquart, B.: High-resolution fourier transform measurement of the no2 visible and near-
513 infrared absorption cross sections: Temperature and pressure effects, 107,
514 10.1029/2001JD000971, 2002.

515

516 Voigt, S., Orphal, J., Bogumil, K., and Burrows, J. P.: The temperature dependence (203–293 k)
517 of the absorption cross sections of o3 in the 230–850 nm region measured by fourier-transform
518 spectroscopy, 143, http://dx.doi.org/10.1016/S1010-6030(01)00480-4, 2001.

519

520 Washenfelder, R. A., Flores, J. M., Brock, C. A., Brown, S. S., and Rudich, Y.: Broadband
521 measurements of aerosol extinction in the ultraviolet spectral region, Atmos. Meas. Tech., 6,
522 10.5194/amt-6-861-2013, 2013.

523

524 Weingartner, E., Saathoff, H., Schnaiter, M., Streit, N., Bitnar, B., and Baltensperger, U.:
525 Absorption of light by soot particles: Determination of the absorption coefficient by means of
526 aethalometers, 34, http://dx.doi.org/10.1016/S0021-8502(03)00359-8, 2003.

527

528

529

530